



## Study of the synthesis of CeO<sub>2</sub> nanoparticles for their use in CO preferential oxidation (COPrOx)



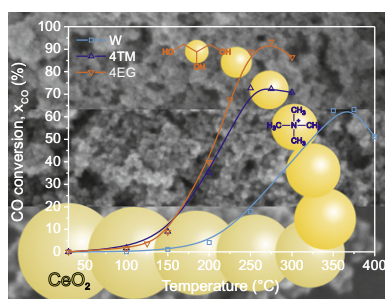
Leonardo F. Peiretti, Inés S. Tiscornia, Eduardo E. Miró\*

Instituto de Investigaciones en Catálisis y Petroquímica, INCAPE (FIQ, UNL – CONICET), Argentina

### HIGHLIGHTS

- Ceria nanoparticles were synthesized by a simple, easy to scale-up method.
- The effect of EG and TMAH on particle and crystallite size was studied.
- Complete elimination of nitrates and organic matter could be achieved at 500 °C.
- The activity of ceria nanoparticles in COPrOx depends on calcination temperature.
- Samples pretreated at 500 °C presented high conversions at the lowest temperature.

### GRAPHICAL ABSTRACT



### ARTICLE INFO

#### Article history:

Received 22 November 2012  
Received in revised form 19 February 2013  
Accepted 27 February 2013  
Available online 8 March 2013

#### Keywords:

Ceria nanoparticles  
Heat treatment  
Ethylene glycol  
TMAH  
COPrOx

### ABSTRACT

CeO<sub>2</sub> nanoparticles were synthesized by the controlled precipitation method from a Ce(NO<sub>3</sub>)<sub>3</sub> solution. To this end, two additives were used alternatively: ethylene glycol (EG) and tetramethylammonium hydroxide (TMAH). Their function was to reduce the particle size obtained after the synthesis. After precipitation and drying, nitrate and organic residuals must be removed, and the method employed for this step could affect the structure and size of the particles. This is an important issue for achieving contaminant-free measurements in catalytic tests. In order to optimize the residuals removing process, a thorough study of the species present and/or eliminated was carried out. Our findings show that a calcination temperature of at least 500 °C is necessary in order to accomplish the complete removal of solvent and precursors such as NO<sub>3</sub><sup>-</sup>. Among the catalysts studied, the one prepared with EG showed the best activity for CO preferential oxidation. In order to study the effect of the residuals upon the catalytic activity, samples prepared using EG were calcined at different temperatures and tested for the COPrOx reaction. CO conversions for all the samples were between 80% and 93% at different temperatures. The best activity was obtained with the sample calcined at 500 °C, which is in agreement with the minimum temperature necessary for the total elimination of residuals.

© 2013 Elsevier B.V. All rights reserved.

## 1. Introduction

In recent years, several developments have been carried out based on nanomaterials, i.e. materials with a 1–100 nm size range, e.g. particles of different shapes (polyhedral, spheres, rods, tubes, needles and tunable forms), films, or nanodots. Within this size

range, these materials show peculiar properties that can be adequately used in numerous applications. Ceria nanoparticles obtained from different synthesis techniques have been extensively studied for their potential use in many applications. Hydrothermal synthesis [1,2], microemulsion [3,4], sol–gel [5], microwave-assisted [6,7] and controlled precipitation [8–11] are some of the methods allowing their production with a tailored-made control of their size and shape. The controlled precipitation technique is very attractive due to the several advantages it presents, namely, it is a simple, easy to scale-up process with low costs.

\* Corresponding author. Address: Santiago del Estero 2829, (S3000AOM) Santa Fe, Argentina. Tel.: +54 0342 4536861; fax: +54 0342 4536861x14.

E-mail address: [emiro@fiq.unl.edu.ar](mailto:emiro@fiq.unl.edu.ar) (E.E. Miró).

Several recent publications on the production of ceria nanoparticles focus on the study of synthesis variables in order to direct the synthesis towards different morphologies and sizes [12,13]. The elimination of solvent remains from the final product is a very important step in order to obtain representative results on catalytic tests. These remains may skew the gas measurements by their decomposition. To the best of our knowledge, only a few studies have been published addressing the characterization of the species evolution during the removal of solvents or precursors after nanoparticle synthesis and their possible influence on the catalytic reaction behavior. These studies have been frequently conducted for micro and mesoporous materials, but not for nanoparticles and their objectives have been diverse, from crystal size conservation [14] to the achievement of a crystalline structure with uniform porosity [15–17], both of them by template removal.

Ceria nanoparticles have a wide range of applications in different fields. One of the most important recent applications is the Carbon Monoxide Preferential Oxidation (COPrOx), but only as a support or promoter. This reaction decreases the CO concentration at values <10 ppm in the output current from the Water Gas Shift Reaction (WGSr). Otherwise, the Proton Exchange Membrane fuel cell (PEM) poisons itself and cannot produce electric current from H<sub>2</sub> and O<sub>2</sub>. This process of WGSr followed by COPrOx is one of the most promissory for H<sub>2</sub> production. Several catalysts for CO elimination in currents rich in H<sub>2</sub> are under study: Co<sub>3</sub>O<sub>4</sub>/ZrO<sub>2</sub> [19], CoO<sub>x</sub>/CeO<sub>2</sub> [20,21], CuO<sub>x</sub>/CeO<sub>2</sub> [22,23], Pt/CeO<sub>2</sub> [24]. In all cases, well-defined synthesis conditions and pretreatments are necessary for the correct interpretation of the catalytic behavior and support effects. When nanoparticles are prepared, the strict control of synthesis conditions becomes critical. Size reduction has brought about some benefits, like the increase of the effective area and new properties associated with the increasing surface-to-volume ratio. Ceria is widely employed as support or additive in catalysts for COPrOx because of its high oxygen storage capacity and redox activity. It has been mentioned in the literature that the bare oxide has a null or very low activity in COPrOx. Maciel et al. [25] obtained ceria (not nanosized) by two different methods: precipitation and hydrothermal synthesis and showed that pure CeO<sub>2</sub> presented a small conversion of CO to CO<sub>2</sub> at all reaction temperatures (ca. 5%). They also showed that, no matter the method used for synthesis, the CO conversion is very similar. Woods et al. [21] reported that the CO conversion over pure CeO<sub>2</sub> nanoparticles was substantially lower than on the 10% CoO<sub>x</sub>/CeO<sub>2</sub> catalyst (34% at 200 °C against 100% at 175 °C). Marbán and Fuertes [26] also observed that the bare CeO<sub>2</sub> is almost inactive up to 250 °C for this reaction. Thus, cerium oxide has been referred to be either a good support or additive, but no attention has been paid to its intrinsic activity.

In this work, we demonstrate that bare cerium oxide may show interesting catalytic properties towards the COPrOx reaction if synthesis conditions are carefully selected. CeO<sub>2</sub> nanoparticles were synthesized by the controlled precipitation method by adding solvents or salts so as to improve size reduction and monodispersion, properties highly related with nanoparticles. Ethylene glycol (EG) [27] and tetramethylammonium hydroxide (TMAH) [28] were used for this purpose in this synthesis. The effect of both additives on the final product was studied by TGA (Thermogravimetric Analysis) and FTIR (Fourier Transform Infrared) measurements. Our aim was to evaluate the species present in CeO<sub>2</sub> nanoparticles after calcination, trying to elucidate if solvent and counterions can be conveniently eliminated by thermal treatment. Finally, catalytic studies were performed using the samples prepared with EG in the COPrOx reaction in order to evaluate if the species present (precursors remaining after synthesis) influence the performance of the catalyst in the COPrOx. The samples were calcined at different temperatures (key temperatures obtained from TGA/FTIR studies).

## 2. Experimental

### 2.1. Materials

Cerium nitrate [Ce(NO<sub>3</sub>)<sub>3</sub>·6H<sub>2</sub>O, 99%] and a TMAH aqueous solution [(CH<sub>3</sub>)<sub>4</sub>N(OH), 1.0 M ± 0.02 M] from Sigma–Aldrich® and ammonium nitrate (28–30%), EG (≥99.5%), ethanol (99.5%) from Cicarelli® were used without further purification. A solution of EG/H<sub>2</sub>O 70% (V/V) [27] was prepared to dissolve the precursors and obtain the precursor solutions in some samples. The precipitant (NH<sub>4</sub>OH) aqueous solution concentration was ≈3 M. An exact concentration value was not necessary because the alkaline solution was used to maintain the precipitation medium at a pH close to 10.

The CeO<sub>2</sub> Nyacol® powder was obtained by evaporation of this commercial suspension consisting of particles of about 10–20 nm, stabilized in an aqueous acetic acid solution.

### 2.2. Preparation of nanoparticles

Nanoparticles of CeO<sub>2</sub> were synthesized by the controlled diffusion precipitation mechanism [29]. Fig. 1 illustrates the procedure followed to elaborate them. The precursor concentration was 0.2 M for all samples. The precursor solution was always added to NH<sub>4</sub>OH under vigorous stirring. This process was carried out by a syringe pump at a speed of ca. 2 mL/min [30]. Room temperature was selected for the synthesis and ageing steps because it has been reported in the literature that low temperature favors the obtention

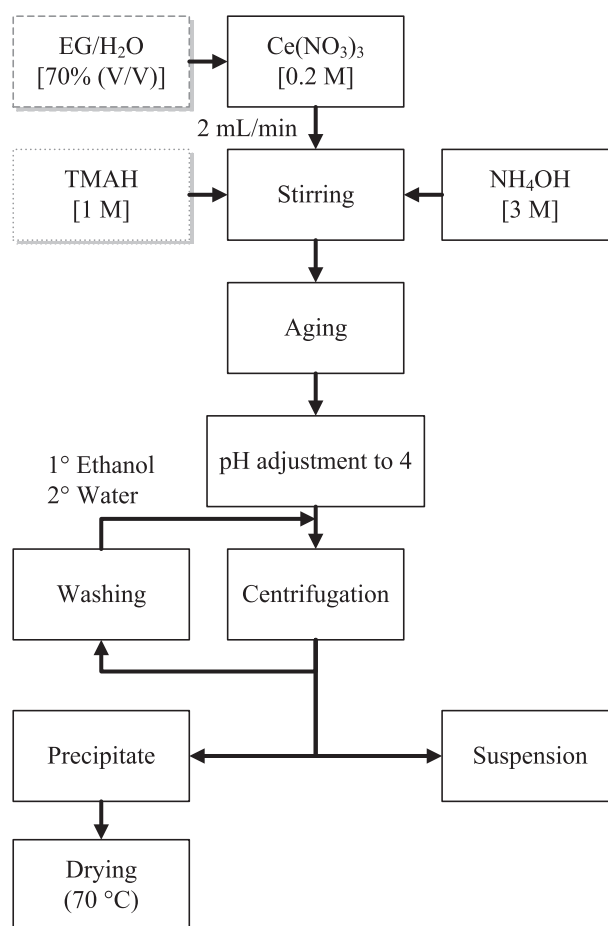


Fig. 1. Block diagram of the experimental procedure. (a) Synthesis with EG; and (b) synthesis with TMAH.

**Table 1**  
Samples prepared and solvents/species present during synthesis.

Sample	pH	Species/solvents used
W	≈7	NH <sub>4</sub> NO <sub>3</sub> , H <sub>2</sub> O, EtOH
4TM	4	NH <sub>4</sub> NO <sub>3</sub> , H <sub>2</sub> O, EtOH, TMAH
4EG	4	NH <sub>4</sub> NO <sub>3</sub> , H <sub>2</sub> O, EtOH, EG
10EG	10	NH <sub>4</sub> NO <sub>3</sub> , H <sub>2</sub> O, EtOH, EG
10TM	10	NH <sub>4</sub> NO <sub>3</sub> , H <sub>2</sub> O, EtOH, TMAH

of small particle sizes [11]. Five samples were synthesized: W, 4TM, 10TM, 4EG, 10EG. The species present and the solvents used are listed in Table 1. Only W was prepared by adding, dropwise, the precursor aqueous solution on the NH<sub>4</sub>OH solution without adjusting the pH after the ageing step (final pH ≈ 7). For the samples 4EG and 10EG, the precursor solution was prepared by dissolving Ce(NO<sub>3</sub>)<sub>3</sub> in the EG/H<sub>2</sub>O solution. For 4TM and 10TM, the Ce(NO<sub>3</sub>)<sub>3</sub> solution was aqueous but, before the syringe pump started to work, 5 mL of TMAH solution were added into the alkaline medium. The concentration choice of this solvent was made according to the smaller particle size obtained with different alcohols and concentrations as reported by Chen and Chang [27]. pH adjustment to 4 and 10 was made with diluted HNO<sub>3</sub> or NH<sub>4</sub>OH and the adopted values were taken from a previous work [30].

The centrifugation of samples was made at 3000 rpm for 15 min. Clean supernatants were obtained for each step (Fig. 1) and, therefore, discarded based on a Dynamic Light Scattering (DLS) measure (not shown) that showed no significant concentration of particles. Particles in suspension remained over the typical precipitate only in the last centrifugation. This suspension was collected and the particles at the bottom were dried at 70 °C overnight in order to analyze them.

### 2.3. Characterization

The solid samples obtained were analyzed by X-ray Diffraction (XRD), Thermogravimetric Analysis (TGA), Fourier Transform Infra-red Spectroscopy (FTIR), Laser Raman Spectra (LRS), Brunauer–Emmett–Teller (BET) nitrogen adsorption isotherms to calculate specific surface area, and Transmission Electron Microscopy (TEM), while supernatants were characterized by Scanning Electron Microscopy (SEM) and Dynamic Light Scattering (DLS).

Crystallite size and crystal structure were determined with a Shimadzu® X-ray diffractometer XD-D1 model, equipped with an X-ray source of Cu Kα (λ = 0.154056 nm) at 30 kV and 40 mA. The first parameter was estimated by the Scherrer equation, and the calculation was performed using the legacy software. The Scherrer constant adopted was 0.9.

The thermogravimetric study was performed in a Mettler Toledo® TGA, TGA/SDTA851<sup>e</sup> model, with a heating rate of 10 °C/min

and an air flow of 60 mL/min. The temperature range was from 30 to 500 °C.

The species present on the dried and calcined samples were determined with a Shimadzu® FTIR spectrometer, IRPrestige-21 model. All samples were diluted in KBr.

Specific surface areas were obtained with a TRISTAR 3000 surface area and porosity measurement instrument from Micromeritics®. Samples were previously evacuated at 200 °C for 8 h under vacuum. Adsorption isotherms were determined by N<sub>2</sub> adsorption over the samples at 77 K. BET surface area was calculated by applying the BET equation to the adsorption isotherms.

Laser Raman measurements of the solids precipitated were performed on a Witec, alpha 300 R Confocal Raman Microscope (CRM) with a green laser source of 532 nm.

The TEM measure of the precipitate were performed on a FEI® transmission electron microscope, Tecnai T20 model with an electron source of 200 kV. Microphotographs of the supernatants were taken on a Carl Zeiss® scanning electron microscope, SUPRA® 40 model with an EHT (electron high tension) of 10.00 kV.

For the DLS measurements, a general-purpose laser light-scattering photometer (from Brookhaven Instruments, Inc.) was fitted with a vertically-polarized He–Ne laser (λ = 632.8 nm), and a digital correlator (model BI-2000 AT). The measurements were carried out at 30 °C.

All characterization techniques, excluding TGA, DLS, were performed at room temperature.

### 2.4. Catalytic tests

Preferential CO oxidation experiments were performed in a fixed-bed flow reactor. Samples were placed in a tubular quartz reactor (6 mm i.d.). The reaction mixture consisted of CO 1%, O<sub>2</sub> 1% and H<sub>2</sub> 40%, He balance. The weight/total flow ratio was adjusted to 2.1 mg cm<sup>-3</sup> min by means of mass flow controllers. The CO conversion and the selectivity towards CO<sub>2</sub> were defined as:

$$x_{\text{CO}} = \frac{[\text{CO}]^0 - [\text{CO}]}{[\text{CO}]^0} \times 100\% \quad (1)$$

$$S_{\text{CO}_2} = \frac{1}{2} \frac{[\text{CO}]^0 - [\text{CO}]}{[\text{O}_2]^0 - [\text{O}_2]} \times 100\% \quad (2)$$

where [CO], and [O<sub>2</sub>] were reactor exit concentrations and [CO]<sup>0</sup>, [O<sub>2</sub>]<sup>0</sup> represented feed concentrations, which were measured with a chromatograph GC-2014 Shimadzu® equipped with a TCD cell.

**Table 2**  
Characteristic sizes of cerium oxide nanoparticles and their catalytic performance in the COPrOx reaction.

Sample	Supernatant		Crystallite			
	SEM (particle (nm))	DLS (agglomerates (nm))	XRD after drying (crystallite (nm))	XRD after reaction (crystallite (nm))	Temperature at x <sub>CO</sub> = 50% (°C)	Selectivity at x <sub>CO</sub> = 50% (%)
W	6.1	127	7.8	9.5	324	48
4TM	7.2	161	6.5	7.0	219	61
4EG	6.7	177	6.0	7.8	208	86
10EG	–	360	7.8	–	–	–
10TM	–	Unstable	9.1	–	–	–
Nyacol®	–	10–20 <sup>a</sup>	4.1	8.3	266	29
4EG (500 °C)	–	–	5.5	6.3	188	87
4EG (450 °C)	–	–	5.5	11.4	218	81

<sup>a</sup> Reported by the manufacturer.

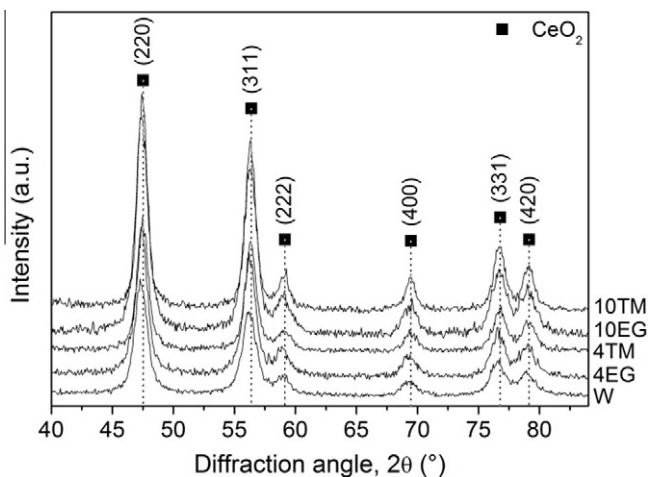


Fig. 2. XRD of ceria nanoparticle samples.

### 3. Results and discussion

#### 3.1. Crystal structure, crystallite and particle size

In general, Table 2 and Fig. 3 show that sizes measured by XRD, SEM and TEM are similar. After reaction, which implies a thermal treatment, the size slightly increases probably due to the rearrangement of atoms induced by heat. This last effect will be further discussed in Section 3.3.2.

Regarding to the crystalline structure, the XRD analysis shows the  $\text{CeO}_2$  characteristic peaks from the cubic fluorite in all the powders precipitated (Fig. 2). Using the Scherrer equation and diffractometer legacy software, crystallite size was determined against a Si standard to correct the profile breadth inherent to the diffractometer (Jones's correction). All the samples prepared were of nanometric size (<100 nm). The results are summarized in Table 2.

Supernatants of the W, 4EG and 4TM samples obtained at the last centrifugation step were characterized by SEM (Fig. 3A). The result obtained for sample 4EG is in agreement with a TEM observation (Fig. 3B). At nanometric scale, a considerable agglomeration can be seen in the samples analyzed (Fig. 3A). Remains of solvents/salts and attraction forces due to particle size may be the cause of this phenomenon. These images show that all the samples have similar mean particle size (Table 2). This implies that the additive used to minimize particle size would not affect the morphology or the mean diameter. On the other hand, EG does minimize the crystallite size of the precipitated solid compared with TMAH. Similar results were obtained by Chen and Chang [27] and Sreeremya et al. [18]. Both of them obtained the same particle size measured by Transmission Electron Microscopy (3.7 nm) using similar EG concentrations. Differences between crystallite and particle size allow us to assume that the centrifugation process could have achieved a particle separation with a mean diameter about 6 nm. Although crystallite size is the minimum size of a particle, the following conclusion can be made concerning the precipitate: the shorter length of the crystal net of  $\text{CeO}_2$  and the similar size observed by SEM, when EG is used as medium of reaction, would indicate that nucleation is more homogeneous. This is consistent with the fact that nucleation begins by setting crystallite size to later increase particle size.

It is interesting to note that crystallite sizes for the same additive are similar for both pH values, 4 and 10. Therefore, the precipitation medium and its effect on nucleation through diffusion control are determining factors for crystallite size [29]. The diffusion control is achieved by either increasing the particle–particle

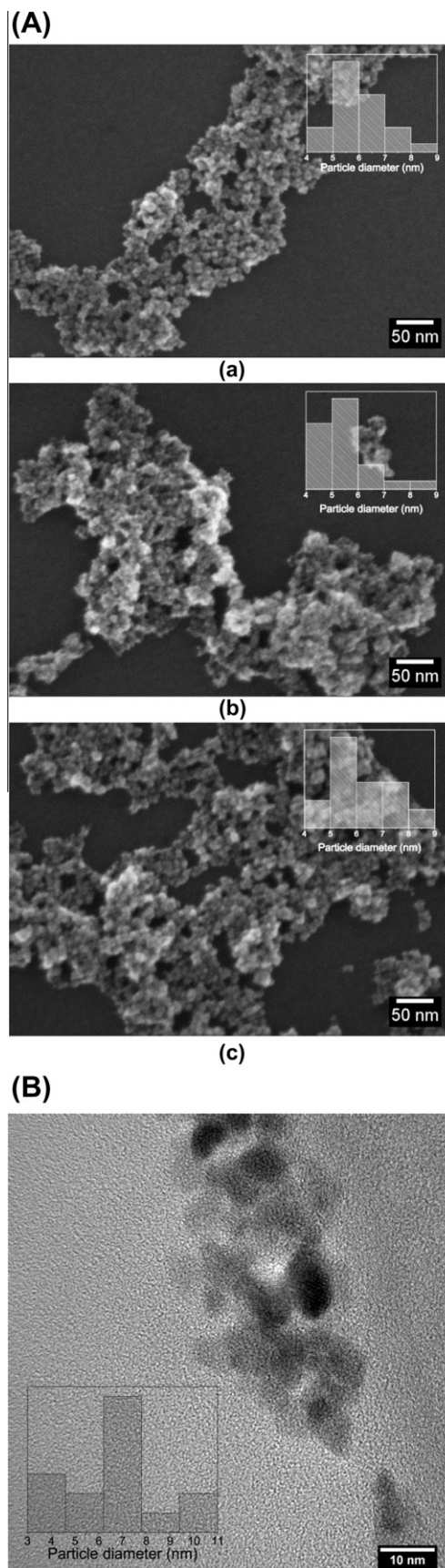
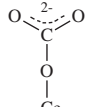
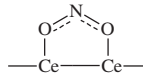


Fig. 3. (A) SEM photographs of  $\text{CeO}_2$  samples. (a) W; (b) 4EG; and (c) 4TM. (B) TEM image of 4EG.

**Table 3**  
FTIR peaks assignment for W, 4EG and 4TM samples.

Species	Assignment (cm <sup>-1</sup> )	References
—OH (superficial)	3400	[33]
—CH <sub>3</sub>	2922 2852	[32]
H <sub>2</sub> O (physisorbed)	1627	[34]
Carboxylic acid [(COO <sup>-</sup> ) <sub>2</sub> ]	1558	[41]
 (Monodentate/polydentate carbonate)	1470 (poly)/≈1500 (mono) 1340 1060	[33,34]
—Ce—		
O <sub>2</sub> <sup>-</sup> (superoxide)	1157	[33,34]
NO <sub>3</sub> <sup>-</sup> (free)	1382	[36]
 (Bridging bidentate nitrite)	1228	[36]
—Ce—		
O <sub>2</sub> <sup>2-</sup> (peroxide)	850	[34]
HC≡CH (di-σ/π-acetylene or di-σ/π-vinylidene)	972	[37]

repulsion during solvent adsorption (EG) or preventing nuclei growing with both steric and charge effects, stronger than those achieved with H<sup>+</sup> (TMAH).

10EG and 10TM samples were discarded from the SEM analysis because their suspension was very unstable at room temperature as can be seen on the DLS measurements (Table 2) and this gives us an idea of a bigger particle size or agglomeration of these samples. At high pH, cohesion between particles is greater, so – even for the 10TM sample – the measurement was difficult to achieve because suspension was very unstable and the agglomerates fell immediately to the bottom of the flask. This fact may hinder and delay heat entrance inside a particle placed at the center of the agglomerate and the escape of gas formed with precursor decomposition. Therefore, for a better understanding of this phenomenon W, 4EG and 4TM samples were selected for the TGA/FTIR study.

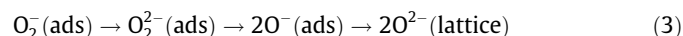
### 3.2. Thermogravimetric analysis (TGA) and precursor decomposition study

In order to gain further insight into the precursor elimination mechanism, TGA experiments were performed. To identify the species present, an FTIR analysis was also made to the calcined samples at selected temperatures. Peak assignments are listed in Table 3.

In all samples, remains of water and ethanol can be seen in the first weight fall (Fig. 4). Their boiling points are both below 100 °C. As it can be observed, an exothermic peak at the Single Differential Thermal Analysis curve (SDTA) appears in all the samples at this stage. At this temperature range, water desorption is a common and endothermic process; therefore, an exothermic reaction must be occurring, overlapping this physical phenomenon. This could be caused by some combustion, probably promoted by the oxidative surface of the CeO<sub>2</sub> nanoparticles, as observed in the progressive elimination of templates [31]. In the FTIR spectra, peaks assigned to —CH<sub>3</sub> groups [32] for the samples dried at 70 °C (Fig. 5) indicate the presence of EtOH, EG or TMAH. The weakness of the signals and the similarities between the FTIR of the three samples at this temperature would indicate that, in the drying step, solvents burned and some decomposition by the superoxide species (O<sub>2</sub><sup>-</sup>) occurred. These species are not stable at room temperature or upon heating at mild temperatures (100 °C) under O<sub>2</sub> pressure [33] as observed in the FTIR spectra (Fig. 5). Peak assignment at ca. 1157 cm<sup>-1</sup> is in agreement with previous studies [33,34].

For all samples, two phenomena can be observed when temperature increases. The first one is the polydentate carbonates (1470 cm<sup>-1</sup>) desorption. Only the monodentate species

(≈1500 cm<sup>-1</sup>) remain on the samples, even at 500 °C as can be seen by FTIR (Fig. 5). The other one is the conversion of superoxide (O<sub>2</sub><sup>-</sup>) into peroxide species (O<sub>2</sub><sup>2-</sup>). As observed, the peak assigned to the first species (1157 cm<sup>-1</sup>) vanishes, while the one at 883 cm<sup>-1</sup> raises its intensity. This reaction can be expressed as follows according to the literature [33,35]:



Previous studies [33,34] have reported that peroxide species can be seen only in H<sub>2</sub> reduced samples of CeO<sub>2</sub>. This may mean that a greater amount of structural defects such as Ce<sup>3+</sup> could be present, providing a greater oxygen adsorption. This might explain why total loss weight is smaller in the W sample compared with 4TM, in which a greater oxidation could have occurred.

On the other hand, the 972 cm<sup>-1</sup> signal could be assigned to acetylene adsorption. This species might appear with additives decomposition since it is not present in the W sample. As reported in the literature [36], two probable adsorption forms could be assigned to this peak (Fig. 6): di-σ/π-acetylene (3000, 1300 and 970 cm<sup>-1</sup>) or di-σ/π-vinylidene (3000, 1450 and 970 cm<sup>-1</sup>). This means that some rests of organic matter remain although in 4EG at 500 °C, the 972 cm<sup>-1</sup> peak practically disappears indicating that removal is almost complete.

#### 3.2.1. W and 4TM samples

The W and 4TM samples exhibited a similar weight loss, which was bigger than 4EG between 30 and 100 °C. This means that the TMAH residual amount is negligible, since the TMAH main decomposition occurs at 134 °C (98% of TMAH decomposes up to 200 °C) [38] and its presence is not observed in the TGA curve or FTIR spectra (CH<sub>3</sub>—N or NH<sub>4</sub><sup>+</sup> groups). In these samples, the presence of NO<sub>2</sub> bridging bidentate groups at 350 °C (Fig. 5a and c) could be due to some partial decomposition of NO<sub>3</sub><sup>-</sup> that starts above 70 °C. Nevertheless, this reaction is endothermic (111.1 kJ/mol [39]); thus, the combustion of rests of solvents or organic salts, as mentioned above, would provide the heat to evaporate water and to start nitrate decomposition above 350 °C.

#### 3.2.2. 4EG sample

First loss weight is minimum in this sample maybe due to the fact that EG increases the water boiling point and, consequently, its desorption temperature. In order to confirm this, a TGA/DTG/SDTA was performed to an EG/H<sub>2</sub>O (70% V/V) solution adsorbed on an inert matrix of amorphous silica (Fig. 7). The analysis was carried out under conditions similar to those of all the above samples: 30–500 °C,

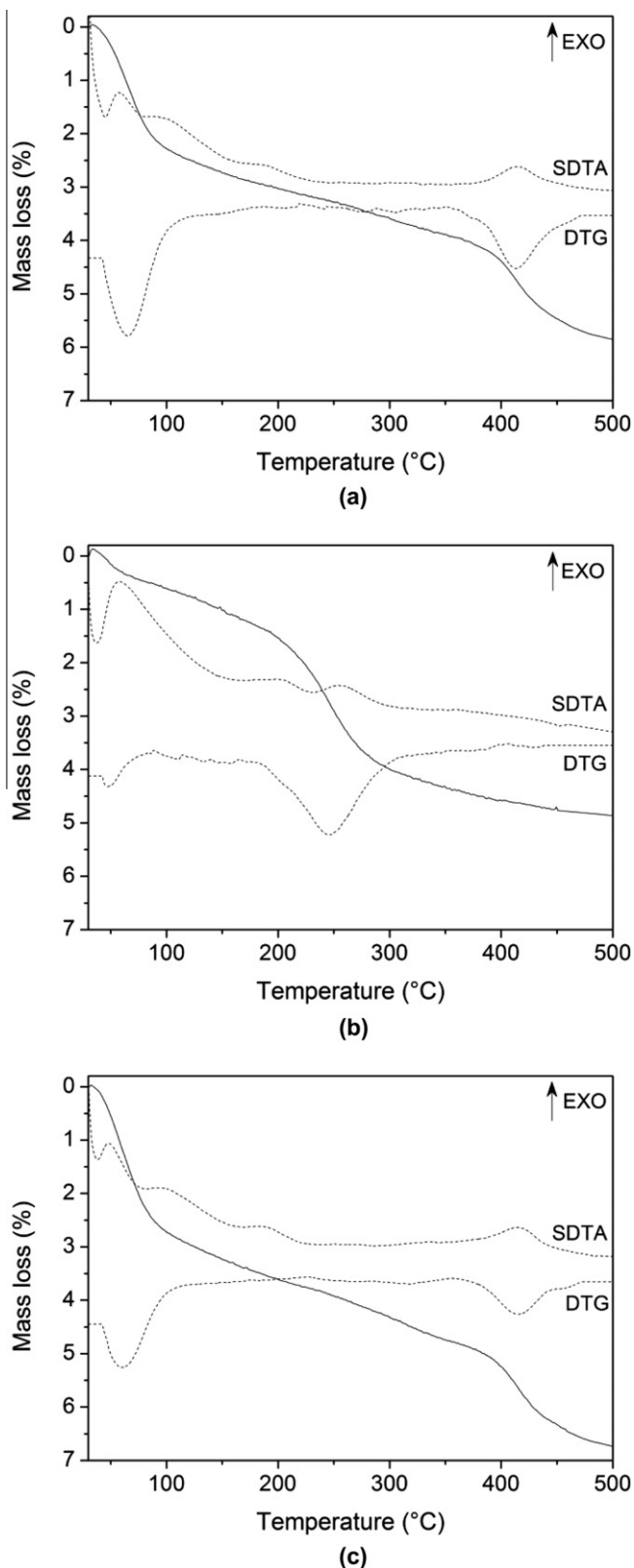


Fig. 4. TGA/DTG/SDTA of samples analyzed. (a) W; (b) 4EG and (c) 4TM.

10 °C/min. Fig. 7 shows the loss weight up to 300 °C only, because no further weight loss was detected above this temperature. An endothermic peak can be observed at ca. 110 °C showing the increase of the water desorption temperature. Another peak at 180 °C can be assigned to EG boiling (195 °C). Returning to the 4EG sample (Fig. 5b),

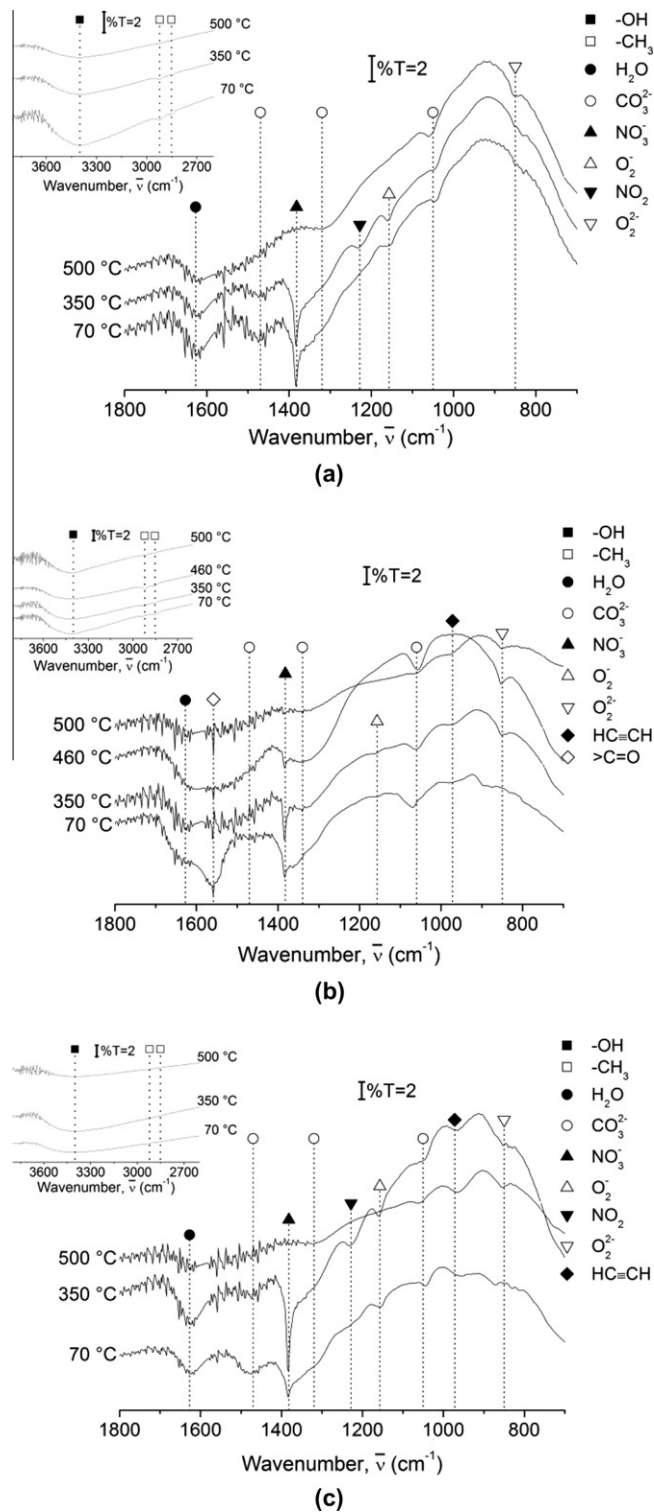


Fig. 5. FTIR spectra at different calcination temperatures for each sample. (a) W; (b) 4EG and (c) 4TM.

the presence of carbonyl groups at 1558  $\text{cm}^{-1}$  indicates EG oxidation to oxalic acid in drying [40]. Moreover, the FTIR peaks belong to doubly negative species according to the literature [41] (signal at 1305  $\text{cm}^{-1}$  is overlapped by carbonate species). This is consistent with the fact that particle surface must be positive since at low pH (high  $[\text{H}^+]$ ) the repulsion forces maintain the size of agglomerates lower than at high pH [42]. Beyond this small weight fall, the signal fading of carbonyl groups indicates that the burning of some oxalic

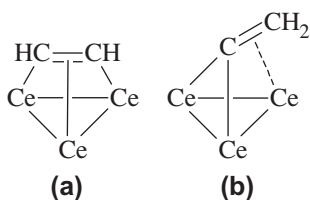


Fig. 6. Acetylene adsorption forms. (a) di- $\sigma/\pi$ -acetylene; and (b) di- $\sigma/\pi$ -vinylidene.

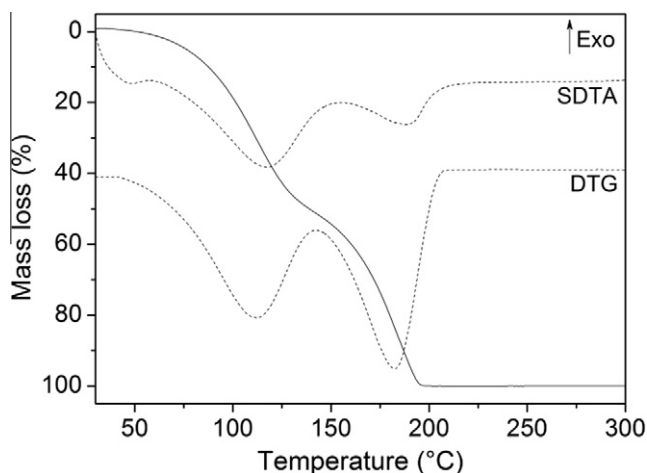


Fig. 7. TGA/DTG/SDTA of EG/H<sub>2</sub>O (70% V/V) over amorphous silica.

acid polymer-like structures could be responsible for the greater weight loss at ca. 250 °C [40].

The NO<sub>2</sub> peaks do not appear on the 4EG FTIR sample. This means that NO<sub>3</sub><sup>-</sup> decomposition produces N<sub>2</sub> through residual organic matter oxidation (exothermic), which is greater on this sample because the polymer-like structure of the oxalic acid.

The appearance of superoxide (O<sub>2</sub><sup>-</sup>) assigned peaks could be explained in the same way as the 4TM sample. Additives present (EG or TMAH) may hinder the oxygen uptake on precipitation, generating an incomplete oxidation and the presence of Ce<sup>3+</sup> species that produce a greater amount of oxygen vacancies.

In general, the additive incorporation could allow a greater reduction of the crystallite and a controlled narrow size distribution. However, remains of TMAH or solvents like EG or ethanol could affect the available area of the catalyst. Nitrates and organic matter can be eliminated, at least from 500 °C, which can be seen in the absence of methyl peaks on the FTIR spectra of these samples. On the other hand, the thermal treatment at this temperature will inevitably increase crystallite size [43] but, as said above, it does not affect the oxidizing properties of CeO<sub>2</sub>. This is a key issue because the main property of this oxide is its capacity to act as oxygen storage.

### 3.3. COPrOx on CeO<sub>2</sub> nanoparticles

#### 3.3.1. Effect of the method of synthesis

The three samples analyzed by TGA and FTIR (W, 4EG and 4TM) and the commercial Nyacol<sup>®</sup> were tested for CO preferential oxidation in a H<sub>2</sub> rich flow. Before this, the four samples were calcined in air flow by increasing temperature at 2 °C min<sup>-1</sup> up to 500 °C, and maintaining it at this value for 2 h. This temperature was selected based on the results shown above, which indicate that at 500 °C all the samples were clean of precursors or solvents. The results of the tests are presented in Fig. 8. The 4EG sample (Fig. 8a) showed the

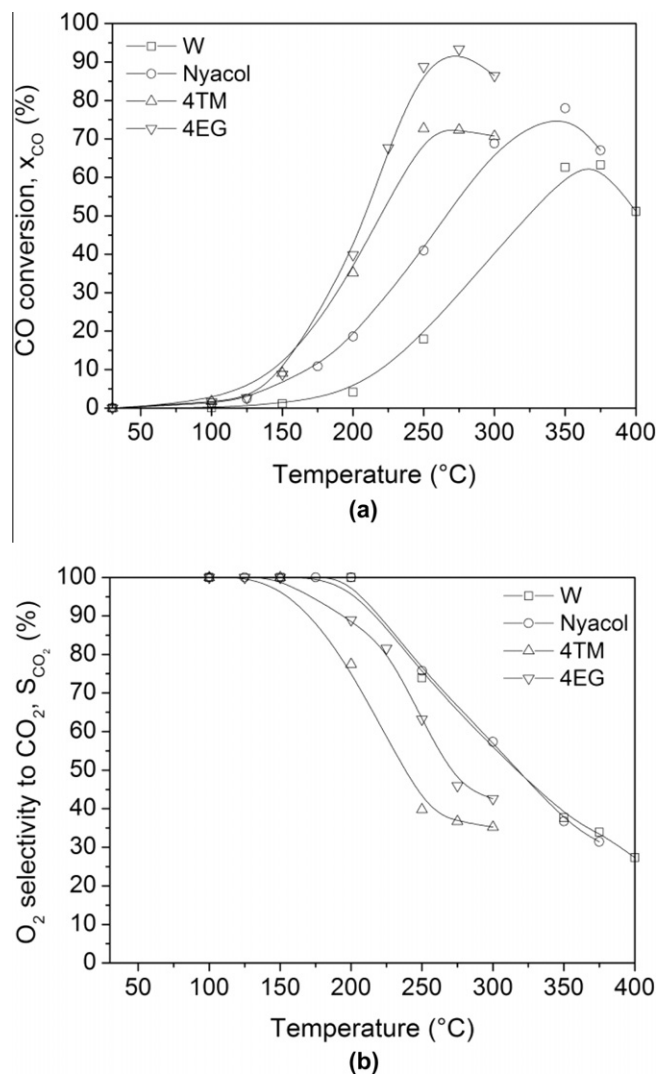


Fig. 8. COPrOx over CeO<sub>2</sub>. (a) CO conversion; and (b) O<sub>2</sub> selectivity to CO<sub>2</sub>.

maximum conversion of CO (93%) at the lowest reaction temperature (275 °C). The 4TM sample presented a lower conversion (72%) at the same temperature as 4EG. The similarity between the CO conversion curves of 4EG and 4TM allows mentioning that the selectivity of O<sub>2</sub> towards CO<sub>2</sub> was also better in the 4EG sample (Fig. 8b). The commercial sample of Nyacol<sup>®</sup> showed conversions lower than 4EG and 4TM, but higher than W. It is interesting to note that its crystallite size (obtained in the same way as the other samples) is the smallest of all samples (4.4 nm). The low CO conversion could be due to the amount of organic matter present in the commercial suspension that produces carbon deposits that poison CeO<sub>2</sub>. However, although the information about the product is not readily available, the relative density of 1.22 and the relative viscosity of 10 for a 20 wt.% suspension allows assuming that the suspension contains an important amount of organic stabilizers. This is not the case of the W sample (see below), which has the lowest CO conversion. The selectivity towards CO<sub>2</sub> of these samples was similar and cannot be compared with that of the 4EG and 4TM samples because the CO conversion curves are different. For example, at 250 °C, the higher selectivity in W (73.9%) is due to the fact that the conversion of CO to CO<sub>2</sub> is just starting (17.9%) while in the 4EG sample it is reaching a higher value (88.8%). Then, it is valid to expect that the selectivity to CO<sub>2</sub> of the 4EG sample will be smaller (63.2%).

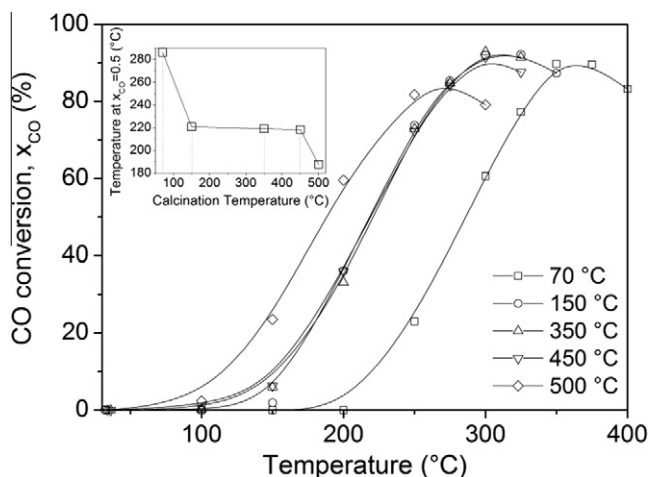


Fig. 9. CO conversion on COPrOx for 4EG calcined at different temperatures.

When samples 4EG, 4TM and W are compared, the first shows a better catalytic performance, probably due to the following properties: the narrower size distribution (Table 2), the mechanism of nitrate elimination that starts at lower temperatures producing nitrogen (cleaner route) and/or the formation of peroxide and superoxide species (Fig. 5B). Organic matter is also eliminated at lower temperatures in the 4EG sample. Therefore, this sample was subjected to a deeper analysis, studying the effect of the calcination temperature upon CO conversion and O<sub>2</sub> selectivity.

### 3.3.2. Effect of calcination temperature upon COPrOx reaction for the samples prepared with EG

In order to determine if calcination temperature and the consequent presence of precursors or solvents affect the CO conversion in the COPrOx, five 4EG samples were calcined at different temperatures in air flow. A new batch of nanometric CeO<sub>2</sub> was prepared at the same conditions used for the 4EG sample, showing an acceptable reproducibility; then, it was divided into five identical samples. The crystallite size obtained after this synthesis (5.2 nm), was somewhat smaller as compared with the one previously prepared (6.7 nm), probably due to small differences in the flow rate regulated by the syringe pump, which establishes some change in the kinetics of precipitation, lowering the Ostwald ripening. Samples were treated at five key temperatures: 70 (dried samples), 150, 350, 450 and 500 °C. These were selected based on TGA/SDTA/FTIR studies (see Figs. 4b and 5b).

CO preferential oxidation results follow the expected tendency. Fig. 9 shows that the temperatures at the maximum CO conversion decrease with the increase of the calcination temperature. The insert in Fig. 9 shows that the temperature at which each sample reaches 50% of CO conversion is practically constant for calcinations between 150 and 450 °C and falls for the sample calcined at 500 °C. It is interesting to observe that at 500 °C, even with the lowest value of the maximum CO conversion, the consumption of CO does not fall at values below 80%, and the statistical range of maximum CO conversions is about 8%. Table 2 summarizes the COPrOx results. The 4EG samples calcined at 500 °C present the lower temperatures at which 50% CO conversion is reached, and the higher O<sub>2</sub> selectivity.

BET measurements performed on the 4EG samples treated at 70 °C and 450 °C, show surface areas of 89.3 m<sup>2</sup>/g and 63.3 m<sup>2</sup>/g, respectively. Thus, the changes in catalytic activity are not due to the changes in surface area. Note that while the sample treated at 70 °C presents 50% of conversion at 280 °C, the sample calcined at 450 °C presents the same conversion at 218 °C. Furthermore, the

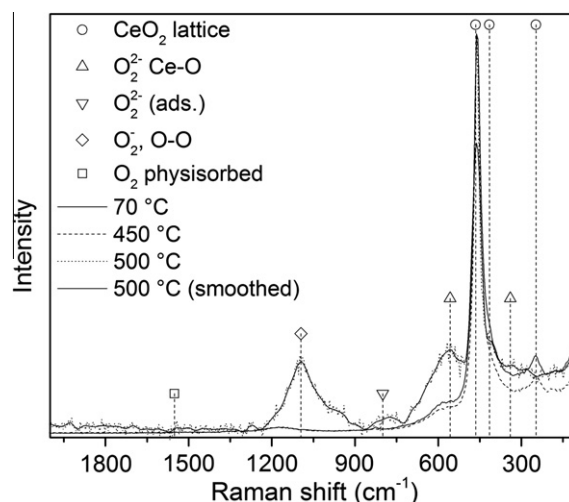


Fig. 10. Laser Raman spectra for samples 4EG pretreated at different temperatures.

decrease in surface area observed is consistent with the increase in crystallite size observed after reaction (Table 2).

In order to gain further insight in the effect of calcination temperature, LRS experiments were performed on 4EG samples pretreated to 70, 450 and 500 °C (Fig. 10). The peaks assignments were based on the work of Pushkarev [35]. It can be clearly seen that, when temperature increases, the signals that correspond to peroxide and superoxide species increase as a consequence of the adsorption of O<sub>2</sub> on oxygen vacancies, as well as the number of defects (Ce<sup>3+</sup>). This tendency may be a consequence of the cleaning of the surface provoked by the residuals elimination after the high temperature treatment. Furthermore, the higher contact time with O<sub>2</sub> in this stage and the higher interatomic distances, for the samples pretreated at higher temperatures, allow a greater O<sub>2</sub> incorporation into the CeO<sub>2</sub> lattice.

Further studies are under way to prepare M-Ce nanoparticle catalysts (M = Cu, Co), in which we will apply our findings to optimize the preparation conditions.

## 4. Conclusions

The thermal decomposition of precursors and solvents after the synthesis of ceria nanoparticles by the controlled precipitation method is a complex process that gives place to the formation of several species adsorbed on the surface of the materials. By combining FTIR and TGA/SDTA techniques, we have characterized the chemical nature of the said species and the temperature ranges at which they evaporated or decomposed. Organic species such as di-σ/π-acetylene and di-σ/π-vinylidene remain on the surface of some of the samples at temperatures near 500 °C together with different types of carbonates and nitrates, indicating that at least this temperature is necessary to obtain non-contaminated ceria nanoparticles. The process of nitrates and organic matter elimination could affect the structure and size of the particles. Therefore, the analysis reported in this work may contribute to gain further insight into the field of nanoparticle synthesis.

The findings obtained in this work about synthesis procedures were reflected in the behavior of the COPrOx reaction. The sample that showed better CO conversion and O<sub>2</sub> selectivity was the one prepared at pH = 4, preparing the precursor by dissolving Ce(NO<sub>3</sub>)<sub>3</sub> in an EG/H<sub>2</sub>O solution (sample 4EG). This sample showed a narrower size distribution and a cleaner mechanism of elimination of nitrates that starts at lower temperatures producing only nitrogen. Moreover, organic matter was also eliminated at lower



temperature for this sample. Note that in the 4EG sample the best results for the COPrOX reaction were obtained with the sample calcined at 500 °C, which is the key temperature at which precursors and intermediates were eliminated, as shown in FTIR and TGA/SDTA experiments.

## Acknowledgments

The authors wish to acknowledge the financial support received from UNL, ANPCyT and CONICET. Thanks are given to Elsa Grimaldi for the English language editing, to Luis Gugliotta for his assessment of the DLS technique, to María Claudia Marchi for the SEM microphotographs and to Hung-Yi Chang for helpful discussions on the synthesis technique. Thanks are also given to the INA (Instituto de Nanociencia de Aragón, Spain) for the supplementary measurements.

## References

- [1] F. Lu, F. Meng, L. Wang, J. Luo, Y. Sang, Morphology-selective synthesis method of nanopolyhedra and square-like CeO<sub>2</sub> nanoparticles, *Mater. Lett.* 73 (2012) 154–156.
- [2] C.A. Orge, J.J.M. Órfão, M.F.R. Pereira, A.M. Duarte de Farias, R.C. Rabelo Neto, M.A. Fraga, Ozonation of model organic compounds catalyzed by nanostructured cerium oxides, *Appl. Catal. B* 103 (2011) 190–199.
- [3] E. Kockrick, C. Schrage, A. Grigas, D. Geiger, S. Kaskel, Synthesis and catalytic properties of microemulsion-derived cerium oxide nanoparticles, *J. Solid State Chem.* 181 (2008) 1614–1620.
- [4] K. Nagy, I. Dékány, Preparation of nanosize cerium oxide particles in W/O microemulsions, *Colloids Surf. A* 345 (2009) 31–40.
- [5] S. Gnanam, V. Rajendran, Synthesis of CeO<sub>2</sub> or  $\alpha$ -Mn<sub>2</sub>O<sub>3</sub> nanoparticles via sol-gel process and their optical properties, *J. Sol-Gel Sci. Technol.* 58 (2011) 62–69.
- [6] E.K. Goharshadi, S. Samiee, P. Nancarrow, Fabrication of cerium oxide nanoparticles: characterization and optical properties, *J. Colloid Interface Sci.* 356 (2011) 473–480.
- [7] S. Samiee, E.K. Goharshadi, Effects of different precursors on size and optical properties of ceria nanoparticles prepared by microwave-assisted method, *Mater. Res. Bull.* 47 (2012) 1089–1095.
- [8] C.J. Shih, Y.J. Chen, M.H. Hon, Synthesis and crystal kinetics of cerium oxide nanocrystallites prepared by co-precipitation process, *Mater. Chem. Phys.* 121 (2010) 99–102.
- [9] S.A. Hassanzadeh-Tabrizi, M. Mazaheri, M. Aminzare, S.K. Sadrnezhaad, Reverse precipitation synthesis and characterization of CeO<sub>2</sub> nanopowder, *J. Alloys Compd.* 491 (2010) 499–502.
- [10] J.-C. Chen, W.-C. Chen, Y.-C. Tien, C.-J. Shih, Effect of calcination temperature on the crystallite growth of cerium oxide nano-powders prepared by the co-precipitation process, *J. Alloys Compd.* 496 (2010) 364–369.
- [11] H.-Y. Chang, H.-I. Chen, Morphological evolution for CeO<sub>2</sub> nanoparticles synthesized by precipitation technique, *J. Cryst. Growth* 283 (2005) 457–468.
- [12] F. Zhou, X. Zhao, H. Xu, C. Yuan, CeO<sub>2</sub> Spherical crystallites: synthesis, formation mechanism, size control, and electrochemical property study, *J. Phys. Chem. C* 111 (2007) 1651–1657.
- [13] S. Kuiry, S. Patil, S. Deshpande, S. Seal, Spontaneous self-assembly of cerium oxide nanoparticles to nanorods through supraaggregate formation, *J. Phys. Chem. B* 109 (2005) 6936–6939.
- [14] E. Mateo, A. Paniagua, C. Güell, J. Coronas, J. Santamaría, Study on template removal from silicalite-1 giant crystals, *Mater. Res. Bull.* 44 (2009) 1280–1287.
- [15] M.J.B. Souza, A.S. Araujo, A.M.G. Pedrosa, S.H. Limab, V.J. Fernandez Jr., Kinetic parameters of surfactant removal occluded in the pores of the AlMCM-41 nanostructured materials, *Thermochim. Acta* 443 (2006) 183–188.
- [16] I. Truijen, A. Hardy, M.K. Van Bael, H. Van den Rul, J. Mullens, Study of the decomposition of aqueous citratoperoxo-Ti(IV)-gel precursors for titania by means of TGA-MS and FTIR, *Thermochim. Acta* 456 (2007) 38–47.
- [17] F. Kleitz, W. Schmidt, F. Schüth, Evolution of mesoporous materials during the calcination process: structural and chemical behavior, *Micropor. Mesopor. Mater.* 44–45 (2001) 95–109.
- [18] T.S. Sreeremya, K.M. Thulasi, A. Krishnan, S. Ghosh, A novel aqueous route to fabricate ultrasmall monodisperse lipophilic cerium oxide nanoparticles, *Ind. Eng. Chem. Res.* 51 (2012) 318–326.
- [19] L.E. Gómez, I.S. Tiscornia, A.V. Boix, E.E. Miró, Co/ZrO<sub>2</sub> catalysts coated on cordierite monoliths for CO preferential oxidation, *Appl. Catal. A* 401 (2011) 124–133.
- [20] C.-W. Tang, M.-C. Kuo, C.-J. Lin, C.-B. Wang, S.-H. Chien, Evaluation of carbon monoxide oxidation over CeO<sub>2</sub>/Co<sub>3</sub>O<sub>4</sub> catalysts: effect of ceria loading, *Catal. Today* 131 (2008) 520–525.
- [21] M.P. Woods, P. Gawade, B. Tan, U.S. Ozkan, Preferential oxidation of carbon monoxide on Co/CeO<sub>2</sub> nanoparticles, *Appl. Catal. B* 97 (2010) 28–35.
- [22] O.H. Laguna, E.M. Ngassa, S. Oraá, A. Álvarez, M.I. Domínguez, F. Romero-Sarria, G. Arzamendi, L.M. Gandía, M.A. Centeno, J.A. Odriozola, Preferential oxidation of CO (CO-PROX) over CuO<sub>x</sub>/CeO<sub>2</sub> coated microchannel reactor, *Catal. Today* 180 (2012) 105–110.
- [23] J.L. Ayastuy, N.K. Gamboa, M.P. González-Marcos, M.A. Gutiérrez-Ortiz, CuO/CeO<sub>2</sub> washcoated ceramic monoliths for CO-PROX reaction, *Chem. Eng. J.* 171 (2011) 224–231.
- [24] O. Pozdnyakova, D. Teschner, A. Wootsch, J. Kröhnert, B. Steinhauer, H. Sauer, L. Toth, F.C. Jentoft, A. Knop-Gericke, Z. Paál, R. Schlögl, Preferential CO oxidation in hydrogen (PROX) on ceria-supported catalysts, part I: Oxidation state and surface species on Pt/CeO<sub>2</sub> under reaction conditions, *J. Catal.* 237 (2006) 1–16.
- [25] C.G. Maciel, T. de Freitas Silva, M.I. Hirooka, M.N. Belgacem, J.M. Assaf, Effect of nature of ceria support in CuO/CeO<sub>2</sub> catalyst for PROX-CO reaction, *Fuel* 97 (2012) 245–252.
- [26] G. Marbán, A.B. Fuertes, Highly active and selective CuO<sub>x</sub>/CeO<sub>2</sub> catalyst prepared by a single-step citrate method for preferential oxidation of carbon monoxide, *Appl. Catal. B* 57 (2005) 43–53.
- [27] H.-I. Chen, H.-Y. Chang, Homogeneous precipitation of cerium dioxide nanoparticles in alcohol/water mixed solvents, *Colloids Surf. A* 242 (2004) 61–69.
- [28] J.Y. Ying, Design and synthesis of nanostructured catalysts, *Chem. Eng. Sci.* 61 (2006) 1540–1548.
- [29] G. Cao, *Nanostructures and Nanomaterials: Synthesis, Properties and Applications*, first ed., Imperial College Press, London, 2004.
- [30] M. Yan, W. Wei, N. Zuoren, Influence of pH on morphology and formation mechanism of CeO<sub>2</sub> nanocrystalline, *J. Rare Earths* 25 (2007) 53–57.
- [31] A.B. Sifontes, G. Gonzalez, J.L. Ochoa, L.M. Tovar, T. Zoltan, E. Cañizales, Chitosan as template for the synthesis of ceria nanoparticles, *Mater. Res. Bull.* 46 (2011) 1794–1799.
- [32] B. Yan, H. Zhu, Controlled synthesis of CeO<sub>2</sub> nanoparticles using novel amphiphilic cerium complex precursors, *J. Nanopart. Res.* 10 (2008) 1279–1285.
- [33] C. Binet, M. Daturi, J.-C. Lavalley, IR study of polycrystalline ceria properties in oxidized and reduced states, *Catal. Today* 50 (1999) 207–225.
- [34] A. Davydov, N.T. Sheppard (Eds.), *Molecular Spectroscopy of Oxide Catalyst Surfaces*, John Wiley & Sons Ltd, 2003.
- [35] V.V. Pushkarev, V.I. Kovalchuk, J.L. d'Itri, Probing defect sites on the CeO<sub>2</sub> surface with dioxygen, *J. Phys. Chem. B* 108 (2004) 5341–5348.
- [36] K.I. Hadjiivanov, Identification of neutral and charged surface N<sub>x</sub>O<sub>y</sub> species by IR spectroscopy, *Catal. Rev. Sci. Eng.* 42 (2000) 71–144.
- [37] C. De La Cruz, Vibrational spectroscopy of model systems for adsorbed species on finely divided metal catalysts, in: D.A. Long, J.M. Griffiths (Eds.), *Handbook of Vibrational Spectroscopy*, vol. 4, John Wiley & Sons, Chichester, 2002, p. 3434.
- [38] I. Tanczos, Gy. Pokol, J. Borsa, T. Tóth, H. Schmidt, The effect of tetramethylammonium hydroxide in comparison with the effect of sodium hydroxide on the slow pyrolysis of cellulose, *J. Anal. Appl. Pyrolysis* 68–69 (2003) 173–185.
- [39] C.A. Strydom, C.P.J. van Vuuren, The thermal decomposition of cerium(III) nitrate, *J. Therm. Anal.* 32 (1987) 157–160.
- [40] D. Zhang, T. Yan, L. Shi, C. Pan, J. Zhang, Ethylene glycol reflux synthesis of carbon nanotube/ceria core-shell nanowires, *Appl. Surf. Sci.* 255 (2009) 5789–5794.
- [41] Y.M. Jung, Characterization of pH-dependent IR spectra of oxalic acid: comparison of self-modeling curve resolution analysis with calculation of IR frequencies, *Bull. Korean Chem. Soc.* 24 (2003) 1410–1412.
- [42] A. Sehgal, Y. Lalatonne, J.-F. Berret, M. Morvan, Precipitation-redispersion of cerium oxide nanoparticles with poly(acrylic acid): toward stable dispersions, *Langmuir* 21 (2005) 9359–9364.
- [43] P. Nachimuthu, W.-C. Shih, R.-S. Liu, L.-Y. Jang, J.-M. Chen, The Study of nanocrystalline cerium oxide by X-ray absorption spectroscopy, *J. Solid State Chem.* 149 (2000) 408–413.